Published in International Journal for Numerical Methods in Engineering 36, issue 24, 4165 - 4183, 1993 1
which should be used for any reference to this work

A STREAMLINE-UPWIND-FULL-GALERKIN METHOD FOR SPACE–TIME CONVECTION DOMINATED TRANSPORT PROBLEMS

P. PERROCHET

Institut d'Aménagement des Terres et des Eaux, Département de Génie rural, Ecole Polytechnique Fédérale de Lausanne, CH-1015 Lausanne, Switzerland

SUMMARY

An original space–time finite element approach for the solution of the diffusion–convection equation is proposed in this paper. A slight manipulation of the differential equation suggests that transient transport problems may in fact be seen as 'steady-state space–time transport problems', accurately and easily soluble by the standard Galerkin technique. However, concerning convective transport involving sharp fronts or coarse discretization, it is shown that implementation of dissipation along space–time trajectories significantly improves the solutions. Classical comparative test problems are run to establish the performances of this method, and to show the limits of the more sophisticated Petrov and Taylor–Galerkin schemes. Evocation of a possible space–time anisotropy generated by usual finite difference time-stepping procedures, as well as comparative analysis of amplification matrices, help to understand the accuracy and the robustness of the proposed approach.

INTRODUCTION

The well-known difficulties encountered in the solution of convection-dominated transport problems by conventional numerical techniques have resulted in two general classes of improved methods during the past two decades. In the first class, the apparent success of early upstream finite difference and finite element methods rely on a step-down of spacial accuracy in the discretization process. In the second class a step-up of temporal and spacial accuracy is the basis of the solution strategies.

Even though the first class methods perform well for certain test problems, they are noted for their smearing and corrupting effects on the results when applied to general multidimensional transient cases. To overcome these difficulties a variety of second class methods have been put forward to deal with such situations. Among others, works such as Leonard,[1] Heinrich and Zienkiewicz,[2] Brooks and Hughes,[3] Donea *et al.*,[4,5] Westerink and Shea[6] provide important perspectives for the development of accurate finite element algorithms.

However, contemporary Petrov and Taylor–Galerkin finite element schemes resulting from this evolution still involve finite difference time-stepping procedures. Such procedures, when associated with standard Galerkin schemes, seem to be responsible to a great extent for the shortcomings mentioned above.[4,5] As a matter of fact the need for optimized Petrov and Taylor–Galerkin methods is created by the adoption of this hybrid 'philosophy' (i.e. finite-element–finite-difference schemes), which pertinence has not been questioned very much in the past. Higher-order truncation errors as well as grid orientation effects (although reduced by the

use of higher-order stencils) remain indeed the major drawbacks of finite difference approximations.[7]

At this point it should be noted that the excellent performances of Petrov and Taylor–Galerkin schemes have been generally demonstrated on rather academical examples (i.e. regular grids, smooth fronts). The last in date $N + 2$ Petrov–Galerkin scheme of Cantekin and Westerink[8] shows significant ameliorations compared to the standard N Galerkin. The question left opened here is whether this rather complex $N + 2$ Petrov–Galerkin algorithm, which yields higher-order polynomial operators, could not be replaced by a standard $N + 1$ Galerkin which would yield operators of the same order. This remark may be of importance given the ease of implementation and the robustness of standard Galerkin schemes on practical meshes. Experimentation of Petrov and Taylor–Galerkin techniques on practical problems, like convective transport in 3-D geophysical flow domains involving coarse meshes or sharp fronts, may show the limits of their applicability. This loss of efficiency can be explained by the fact that the typology and the geometry of elements used in practical meshes often contradict the conditions of success of these contemporary methods (asymmetric perturbations not defined for all types of elements, impossibility to accurately calculate the local optimum upwind parameters, local violations of stability conditions on Courant number, Cr). Since these difficulties seem to originate in the finite difference time-stepping procedures, the development of a generalized Galerkin finite element approach appears justified for practical applications.

The idea of using space–time finite elements, initially proposed by Oden[9] for the treatment of a wave equation, has been successfully applied by researchers to solve diffusion-dominated problems.[10–12] This rigorous and truly consistent technique unifies the treatment of space and time derivatives by direct discretization of the space–time continuum. However, this basic approach has generally remained marginal among the modellers' community, probably due to the fact that standard 'lighter' techniques have always given satisfactory results for diffusion-type problems. In the context of convection-dominated processes it will be shown further on that the usual arguments defending computational economy might be revised for the benefit of robustness and space–time accuracy.

The space–time treatment of diffusion–convection equations is also reported in the literature[13,14] for 2-D (x, t) domains. In these works space–time schemes of the Petrov–Galerkin type are systematically used. They give fair results for convective test problems but remain limited by the condition $Cr < 1$. Moreover they still require the precise (i.e. unpractical) calculation of local upwind parameters. A careful examination of these schemes suggests that the asymmetric Petrov–Galerkin perturbation could be made simpler and more properly redefined. As a matter of fact, Yu and Heinrich[15] generalized their work to 3-D (x, y, t) domains based on the Streamline-Upwind-Petrov–Galerkin[3] (SUPG) concept. Yet, in the original SUPG method, the asymmetric perturbation only takes spacial trajectories (in the plane (x, y)) into account and not the effective space–time trajectories in the 3-D (x, y, t) domain. Consequently, for good accuracy in high convection conditions, the multidimensional scheme proposed by these authors is still subject to the classical limitations (i.e. limited sharpness of fronts, $Cr < 1$). The latter may be effectively eliminated by a generalized finite element approach that really preserves the structure of the SUPG technique in the space–time context. As it will be shown later, this approach is already required for the 2-D (x, t) problem.

Broadly speaking, the space–time finite element approach leads to a 'block' treatment of 4-D differential operators. In doing so it allows to re-write the classical transient diffusion–convection equation under an equivalent 'steady-state' form, with time derivatives being the fourth components of the operators. Therefore, robust standard numerical schemes designed to solve steady-

state (x, y, z) space problems could be used for accurate solutions of 'steady-state' (x, y, z, t) problems.

Following this option, the generalized consistent SUPG technique may be advantageously replaced by a standard Galerkin approach with matching space–time longitudinal diffusivity (i.e. the upwind acting along space–time trajectories). This procedure is a 4-D analogy to what was suggested by Kelly *et al.*[16] for 3-D (x, y, z) steady-state problems. In the space–time domain the longitudinal upwind, ensuring the absence of cross wind dissipation, preserves the sharpness of space–time gradients, and hence the shapes of solute fronts along space trajectories. Moreover the desertion of Petrov–Galerkin asymmetric weighting functions makes the solution algorithm and its comprehension more straightforward. The resulting method which could be called SUFG (Streamline-Upwind-Full-Galerkin) is described below.

SPACE–TIME FORMULATION OF DIFFUSION–CONVECTION EQUATIONS

Consider first the particular case of pure convection generally expressed as

$$\frac{\partial C}{\partial t} = -\mathbf{v}\cdot\nabla C, \quad \mathbf{v} = (v_x, v_y, v_z)^{\mathrm{T}} \tag{1}$$

where $\mathbf{v}$ [m/s] is the space velocity field and C [ ] a solute concentration. Equation (1) indicates that the unknown time variations $\partial C/\partial t$ depend on the scalar product between spacial vectors $\mathbf{v}$ and ∇C and are maximum along flow trajectories when the solute front propagates parallel to $\mathbf{v}$. These obvious remarks belong to common sense when space and time are considered as two distinct domains.

Space–time steady-state formulation

A slight manipulation of equation (1) allows to write

$$\frac{\partial C}{\partial t} + \mathbf{v}\cdot\nabla C = 0 \tag{2}$$

or more synthetically

$$\tilde{\mathbf{v}}\cdot\tilde{\nabla} C = 0, \quad \tilde{\mathbf{v}} = (v_x, v_y, v_z, v_t = 1)^{\mathrm{T}}, \quad \tilde{\nabla} C = (\partial_x C, \partial_y C, \partial_z C, \partial_t C)^{\mathrm{T}} \tag{3}$$

Compared to the classical convection equation (1), equation (3) now clearly expresses the unique condition which governs convection. Space–time trajectories and gradients ($\tilde{\mathbf{v}}$ and $\tilde{\nabla} C$) remain always perpendicular. These two vectors are schematized in Figure 1 in the case of 2-D (x, t) sharp front plug-flow problem. Figure 1 shows the block solution of equation (3) as well as boundary conditions $C(0, t)$ and $C(x, 0)$. The latter corresponding to the usual initial condition (Figure 1(b)). Substitution of $C_t = C_y$, $v_t = v_y$ and $C(0, t) = C(0, y)$ in Figure 1 indicates that the solution of this convective plug-flow problem is similar to the 2-D (x, y) solution presented by Hughes and Brooks[17] to test their space steady-state SUPG technique.

Space–time anisotropy in time-discretization techniques based on finite differences

In numerical schemes associating finite elements and finite differences, space and time are discretized in their respective direction but the space–time velocity field $\tilde{\mathbf{v}}$ cannot be represented continuously. As shown in Figure 2, an artificial space–time anisotropy is created which is very

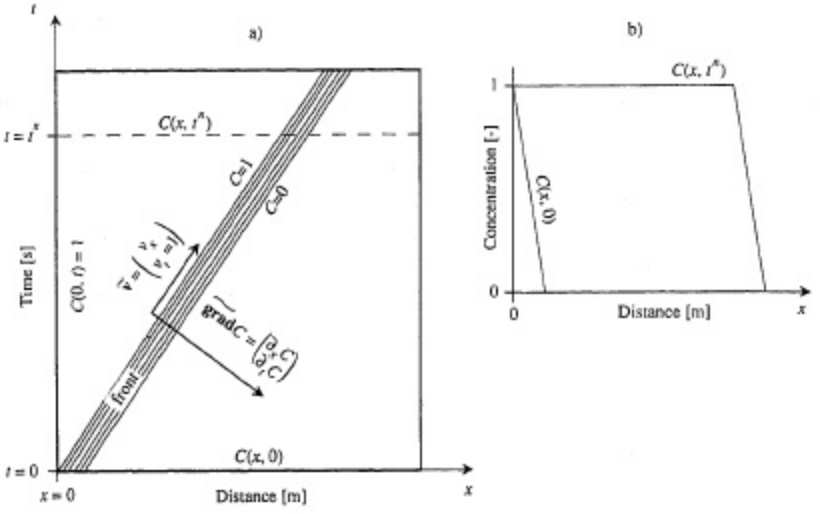

Figure 1. Space–time representation of convection. (a) Function $C(x, t)$ and vectors $\tilde{\mathbf{v}}$ and $\widetilde{\text{grad}}\,C$. (b) Initial condition $C(x, 0)$ and concentration profile $C(x, t^n)$

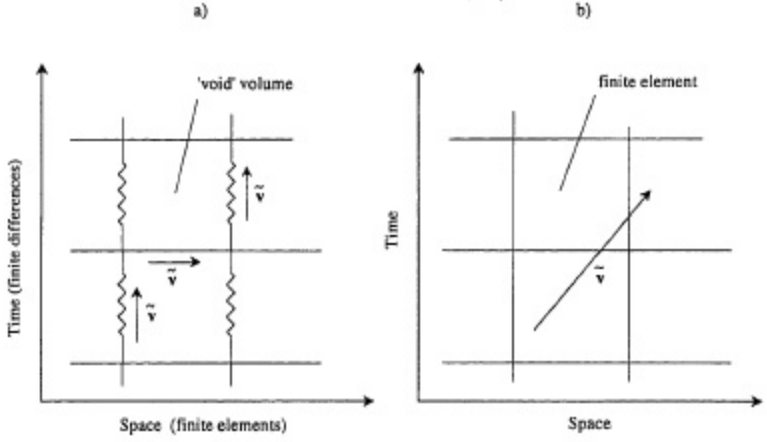

Figure 2. Discontinuous and continuous discretization of the space–time domain. Consequences on the field $\tilde{\mathbf{v}}$. (a) Space–time anisotropy of the usual hybrid techniques. (b) Isotropic finite element representation

analogous to the anisotropy affecting traditional 'resistors networks', where flow is forced horizontally or vertically. Space–time grid orientation effects are similar to those noticed in the finite difference steady-state treatment of the convection equation (see e.g. Reference 7). These effects which are present in most of time-stepping schemes based on finite differences may help to partly explain their limitations when high convection conditions are encountered.

The general diffusion–convection equation can be expressed under the 4-D 'steady-state' form

$$\tilde{\mathbf{V}} \cdot (-\tilde{\mathbf{D}} \tilde{\mathbf{V}} C) + \tilde{\mathbf{v}} \cdot \tilde{\mathbf{V}} C = 0 \tag{5}$$

where $\tilde{\nabla}$ is the 4-D divergence operator and $\tilde{\mathbf{D}}$ the macro-dispersion tensor defined by

$$\tilde{\mathbf{D}} = \begin{bmatrix} & & & 0 \\ & \mathbf{D} & & 0 \\ & & & 0 \\ 0 & 0 & 0 & 0 \end{bmatrix}, \quad \mathbf{D} = \frac{\alpha_L}{\|\mathbf{v}\|}\mathbf{v}\otimes\mathbf{v} + \frac{\alpha_T}{\|\mathbf{v}\|}(\|\mathbf{v}\|^2\mathbf{I} - \mathbf{v}\otimes\mathbf{v}) + D_m\mathbf{I} \tag{6}$$

with α_L and α_T [m] being longitudinal and transverse diffusivities, D_m [m^2/s] the molecular diffusion and $\mathbf{I}$ the identity matrix. In the above equation α_L and α_T refer to the well-known spacial effects of mechanical dispersion (parallel and perpendicular to $\mathbf{v}$) in porous media. However, if these effects are negligible, or if the studied phenomenon does not involve porous material, the two first dispersive terms can be suppressed in equation (6).

Interestingly, for the particular case where $v_x = v_y = v_z = 0$, equation (5) shows that a purely diffusive problem keeps a diffusive–convective structure in the space–time domain. In this case space–time trajectories are simply

$$\tilde{\mathbf{v}} = (0, 0, 0, 1)^T \tag{7}$$

and, $\tilde{\mathbf{v}}$ being always parallel to the time axis, it is apparent that grid orientation effects may be insignificant in diffusive problems.

STREAMLINE-UPWIND-FULL-GALERKIN (SUFG) APPROACH

The space–time generalization of the streamline upwind technique is based on the steady-state (x, y, z) diffusion–convection equation given by Kelly *et al.*[16]

$$\nabla\cdot(-(\mathbf{D} + \bar{\mathbf{D}})\nabla C) + \mathbf{v}\cdot\nabla C = 0 \tag{8}$$

in which $\mathbf{D}$ is defined by equation (6). $\bar{\mathbf{D}}$ is the added diffusivity tensor allowing implementation of the 'anisotropic balancing dissipation', or longitudinal upwind $\bar{\alpha}_L$ [m], acting along flow lines through the tensorial form (see also Reference 16)

$$\bar{\mathbf{D}} = \frac{\bar{\alpha}_L}{\|\mathbf{v}\|}\mathbf{v}\otimes\mathbf{v} \tag{9}$$

For simplicity, and without loss of generality, we consider below the pure convection case with $\mathbf{D} = \mathbf{0}$ ($\alpha_L = 0$, $\alpha_T = 0$, $D_m = 0$) in equation (8). This extreme case is indeed the most difficult to solve numerically. Conversion of equation (8) from space domain (x, y, z) to space–time domain (x, y, t) is achieved by replacing one space variable (here z is chosen) by time variable t through the mapping

$$z = \beta t \tag{10}$$

where β [m/s] is a conversion factor. On the base of (10) follow

$$v_z = \frac{\partial z}{\partial t} = \beta, \quad \frac{\partial C}{\partial z} = \frac{1}{\beta}\frac{\partial C}{\partial t}$$

and

$$\frac{\partial^2 C}{\partial x\,\partial z} = \frac{1}{\beta}\frac{\partial^2 C}{\partial x\,\partial t}, \quad \frac{\partial^2 C}{\partial y\,\partial z} = \frac{1}{\beta}\frac{\partial^2 C}{\partial y\,\partial t}, \quad \frac{\partial^2 C}{\partial z^2} = \frac{1}{\beta^2}\frac{\partial^2 C}{\partial t^2}$$

in Figure 4 and will help to understand the beneficial effects of applying streamline upwinding in the space–time domain.

In the space–time domain there is no boundary layer effects since Neumann conditions are specified on downstream boundaries. Diffusive fluxes are physically zero in the time direction and they are usually specified as such on space boundaries. On the other hand, transient transport of a sharp front generates singularities affecting the concentration profile at a given time level. These singularities are similar to the one shown in Figure 4 for the steady-state (x, y) problem and may be adversely amplified during time stepping. Figure 5 schematically suggests that introduction of the artificial diffusivity $\tilde{\alpha}_L$ tends to smooth out irregularities along space–time trajectories. The sharpness of the front is left intact in this process, at least for very high Pe number problems. For more diffusive problems (low Pe) the artificial tensor $\tilde{\tilde{\mathbf{D}}}$ can actually be suppressed, in which case the SUFG scheme is similar to any standard space–time finite element scheme.

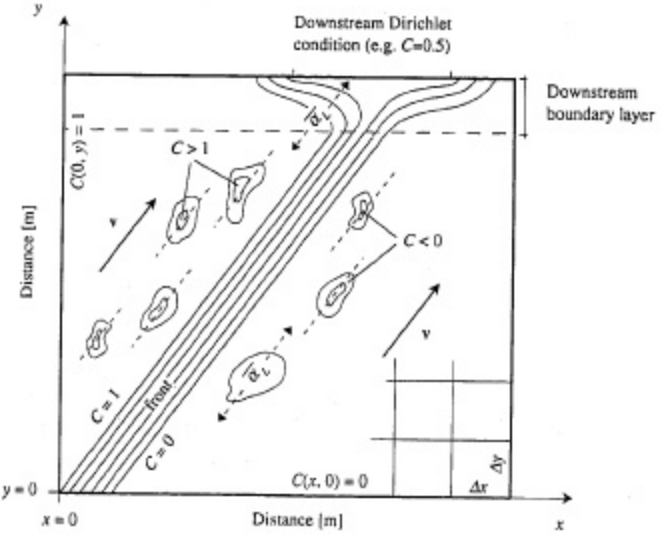

Figure 4. Effects of the spatial longitudinal upwind $\tilde{\alpha}_L$ in steady-state convective transport. Diffusion in the downstream boundary layer and dampening of the singularities $C > 1$ and $C < 0$

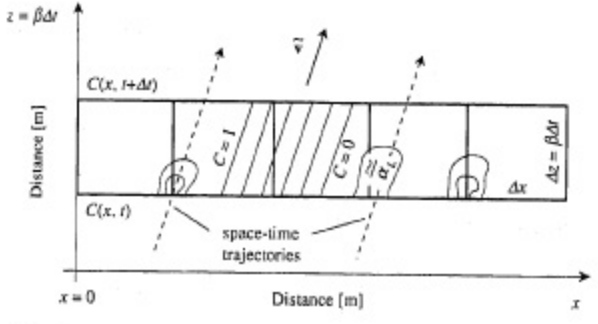

Figure 5. Effects of longitudinal upwind $\tilde{\alpha}_L$. Dampening of singularities along space–time trajectories

The step-by-step growth of errors is governed through time by the amplification matrix of the numerical scheme. This matrix is evaluated further on for the proposed SUFG scheme and its norm is compared with that of the CNG (standard Crank–Nicholson–Galerkin), CNTG[4] (Crank–Nicholson–Taylor–Galerkin), and consistent transient SUPG[3] (Streamline-Upwind-Petrov–Galerkin) schemes. The latter shows an interesting analogy with the SUFG scheme which is discussed below.

Analogy of the SUFG scheme with the transient consistent SUPG scheme

Consider the conventional convection equation

$$\frac{\partial C}{\partial t} = -\mathbf{v}\cdot\nabla C, \quad \mathbf{v} = (v_x, v_y, v_z)^{\mathrm{T}} \tag{17}$$

and multiply both sides (for consistency) by the asymmetric weighting function W_n defined by

$$W_n = N_n + \frac{k}{\|\mathbf{v}\|}\frac{\mathbf{v}}{\|\mathbf{v}\|}\cdot\nabla N_n \tag{18}$$

where k [m^2/s] is the upwind parameter defined for the transient case by minimization of phase errors.[3] As long as the time derivative in equation (17) remains under its exact form, and using the 4-D operator $\tilde{\nabla}$, the resulting equation can be expressed as

$$W_n\tilde{\mathbf{v}}\cdot\tilde{\nabla}C = 0 \tag{19}$$

The consistent SUPG scheme is constructed on the basis of the above equation, time being discretized by central finite differences (Crank–Nicholson), and function W_n being defined by space variables only. By analogy with the steady-state convection equation in the (x, y) plane, expression (19) suggests that artificial (spacial) dissipation could fully be suppressed if oriented in the direction of $\tilde{\mathbf{v}}$ through consistent weighting. However, the SUPG scheme, although low diffusive, cannot achieve the desired effect since the use of finite differences prevents the treatment of tensorial space–time functions. Moreover, to be truly consistent, space–time weighting functions $\tilde{W}_n$ should be used. These restrictive remarks are illustrated further on through simple test examples which show that the SUPG and standard CNG schemes produce results belonging to the same category (downwind slight diffusion, upwind instabilities).

These considerations were sensed by Yu and Heinrich[14,15] in their attempt to extend the SUPG method to the space–time domain (x, y, t). However these authors left out the generalization of the asymmetric perturbation and proposed for the pure convection case*

$$\tilde{W}_n = \tilde{N}_n + \frac{k}{\|\mathbf{v}\|}\left(1 + \Delta t\frac{Cr}{6}\frac{\partial}{\partial t}\right)\frac{\mathbf{v}}{\|\mathbf{v}\|}\cdot\nabla N_n \tag{20}$$

where the original steady-state upwind parameter k is corrected by a function taking into account the time step as well as space–time cross derivatives. Notwithstanding the presence of space–time functions and the apparent complexity of the above perturbation, the upwind parameter in equation (20) clearly acts only along space trajectories defined by $\mathbf{v}$. Hence, the proper generalized streamline upwind effect is not achieved.

Given these basic considerations, a correct space–time generalization of the SUPG method can be obtained by writing equation (19) as

$$\tilde{W}_n\tilde{\mathbf{v}}\cdot\tilde{\nabla}C = 0, \quad \text{with} \quad \tilde{W}_n = \tilde{N}_n + \tilde{k}\frac{\tilde{\mathbf{v}}}{\|\tilde{\mathbf{v}}\|}\cdot\tilde{\nabla}\tilde{N}_n \tag{21}$$

where the parameter $\bar{k}$ [m] corresponds to the space–time added longitudinal diffusivity $\tilde{\bar{\alpha}}_L$ introduced in equation (11). Yet in the proposed SUFG scheme we leave the asymmetric weighting technique and give the preference to the standard (central) Galerkin treatment. The longitudinal upwind (or diffusivity) $\tilde{\bar{\alpha}}_L = \bar{k}$ is then directly introduced in the tensor $\bar{\bar{\mathbf{D}}}$ of matrix equation (15).

Space–time anisotropic diffusivity $\tilde{\bar{\alpha}}_L$ for the SUFG scheme

Given the absence of downstream boundary layers in the space–time domain, the generalization of the spacial quantity $\bar{\alpha}_L$ given by References 16 and 17 is not justified any more. Numerical experiments performed on purely convective (x, t) cases revealed that the apparition of singularities was conditioned by the ratio $v_x \Delta z / \beta \Delta x$ (Courant number), as schematized in Figure 6. However, as a first approximation, the quantity

$$\tilde{\bar{\alpha}}_L = \| \widetilde{\Delta \mathbf{s}} \|, \quad \widetilde{\Delta \mathbf{s}} = (\Delta x, \Delta y, \Delta z = \beta \Delta t)^T \tag{22}$$

was used in these experiments. In definition (22) Δx, Δy, Δz (absolute values) are relative to the discretization (node spacing, element size) in the principal directions. Using bi-quadratic space–time finite elements, stable and wiggle-free solutions (or sometimes with mild residual oscillations) were obtained for $Cr < 2$ (relatively sharp fronts) and $Cr < 4$ (well-diffused initial fronts). As expected, it was noted in these numerical tests that the space–time streamline upwinding process itself was much more important than a precise evaluation of the parameter $\tilde{\bar{\alpha}}_L$.

Moreover, Figure 6 suggests that the classical limitation $Cr \leqslant 1$ affecting contemporary methods can be discarded in the space–time domain. As a matter of fact, the difficulties encountered by the SUFG scheme at high Cr values are essentially related, as in steady-state space simulation, to the interpolation power of the finite elements used (polynomial order of the shape functions). In such situations it is obvious that a more precise evaluation of $\tilde{\bar{\alpha}}_L$ is useless.

Amplification matrix of the SUFG scheme

In order to assess the stabilizing properties of the SUFG scheme, its amplification matrix is constructed below for the purely convective 2-D (x, t) transport. Applying Galerkin's weighted residuals on equation (11) using a bi-linear space–time square element ($\Delta x = \Delta z = \beta \Delta t$) yields the

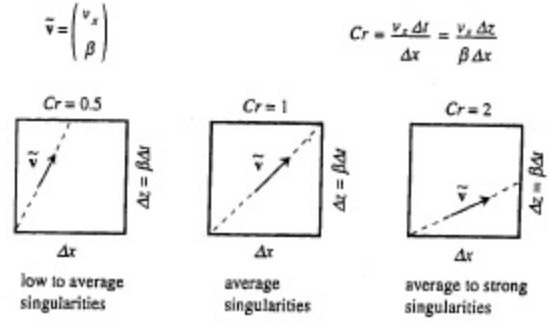

Figure 6. Geometrical interpretation of Courant number (Cr) in the space–time domain

4×4 element matrix equation (15) which becomes after integration

$$\tilde{\mathbf{A}}^e = \frac{\tilde{\alpha}_L}{\|\tilde{\mathbf{v}}\|}\begin{bmatrix} \frac{v_x^2}{3}+\frac{\beta v_x}{2}+\frac{\beta^2}{3} & -\frac{v_x^2}{3}+\frac{\beta^2}{6} & -\frac{v_x^2}{6}-\frac{\beta v_x}{2}-\frac{\beta^2}{6} & \frac{v_x^2}{6}-\frac{\beta^2}{3} \\ * & \frac{v_x^2}{3}-\frac{\beta v_x}{2}+\frac{\beta^2}{3} & \frac{v_x^2}{6}-\frac{\beta^2}{3} & -\frac{v_x^2}{6}+\frac{\beta v_x}{2}-\frac{\beta^2}{6} \\ * & * & \frac{v_x^2}{3}+\frac{\beta v_x}{2}+\frac{\beta^2}{3} & -\frac{v_x^2}{3}+\frac{\beta^2}{6} \\ \text{sym} & * & * & \frac{v_x^2}{3}-\frac{\beta v_x}{2}+\frac{\beta^2}{3} \end{bmatrix}$$

$$+\Delta x\begin{bmatrix} -\frac{v_x}{6}-\frac{\beta}{6} & \frac{v_x}{6}-\frac{\beta}{12} & \frac{v_x}{12}+\frac{\beta}{12} & -\frac{v_x}{12}+\frac{\beta}{6} \\ -\frac{v_x}{6}-\frac{\beta}{12} & \frac{v_x}{6}-\frac{\beta}{6} & \frac{v_x}{12}+\frac{\beta}{6} & -\frac{v_x}{12}+\frac{\beta}{12} \\ -\frac{v_x}{12}-\frac{\beta}{12} & \frac{v_x}{12}-\frac{\beta}{6} & \frac{v_x}{6}+\frac{\beta}{6} & -\frac{v_x}{6}+\frac{\beta}{12} \\ -\frac{v_x}{12}-\frac{\beta}{6} & \frac{v_x}{12}-\frac{\beta}{12} & \frac{v_x}{6}+\frac{\beta}{12} & -\frac{v_x}{6}+\frac{\beta}{6} \end{bmatrix}$$

Substituting $\tilde{\alpha}_L = \|\widetilde{\Delta \mathbf{s}}\| = \sqrt{2}\Delta x$, and considering that $\|\tilde{\mathbf{v}}\| = \beta\sqrt{Cr^2+1}$, $Cr = v_x/\beta$, one obtains after dividing by β and by $\Delta x(=\Delta z)$ the adimensional form

$$\tilde{\mathbf{A}}^e = \sqrt{\frac{2}{Cr^2+1}}\begin{bmatrix} \frac{Cr^2}{3}+\frac{Cr}{2}+\frac{1}{3} & -\frac{Cr^2}{3}+\frac{1}{6} & -\frac{Cr^2}{6}-\frac{Cr}{2}-\frac{1}{6} & \frac{Cr^2}{6}-\frac{1}{3} \\ * & \frac{Cr^2}{3}-\frac{Cr}{2}+\frac{1}{3} & \frac{Cr^2}{6}-\frac{1}{3} & -\frac{Cr^2}{6}+\frac{Cr}{2}-\frac{1}{6} \\ * & * & \frac{Cr^2}{3}+\frac{Cr}{2}+\frac{1}{3} & -\frac{Cr^2}{3}+\frac{1}{6} \\ \text{sym} & * & * & \frac{Cr^2}{3}-\frac{Cr}{2}+\frac{1}{3} \end{bmatrix}$$

$$+\begin{bmatrix} -\frac{Cr}{6}-\frac{1}{6} & \frac{Cr}{6}-\frac{1}{12} & \frac{Cr}{12}+\frac{1}{12} & -\frac{Cr}{12}+\frac{1}{6} \\ -\frac{Cr}{6}-\frac{1}{12} & \frac{Cr}{6}-\frac{1}{6} & \frac{Cr}{12}+\frac{1}{6} & -\frac{Cr}{12}+\frac{1}{12} \\ -\frac{Cr}{12}-\frac{1}{12} & \frac{Cr}{12}-\frac{1}{6} & \frac{Cr}{6}+\frac{1}{6} & -\frac{Cr}{6}+\frac{1}{12} \\ -\frac{Cr}{12}-\frac{1}{6} & \frac{Cr}{12}-\frac{1}{12} & \frac{Cr}{6}+\frac{1}{12} & -\frac{Cr}{6}+\frac{1}{6} \end{bmatrix}$$

The assembly of a layer including n elements, as schematized in Figure 5, yields the $(2n+2)\times(2n+2)$ global matrix $\tilde{\mathbf{A}}$ and the matrix system (16) can be partitioned in

$$\tilde{\mathbf{A}}\mathbf{C} = \begin{bmatrix} \mathbf{AA} & \mathbf{AB} \\ \mathbf{BA} & \mathbf{BB} \end{bmatrix} \begin{pmatrix} \mathbf{C}^t \\ \mathbf{C}^{t+\Delta t} \end{pmatrix} = \mathbf{0} \tag{23}$$

Vector $\mathbf{C}^t$ being the initial condition for the current time step, the $(n+1)\times(n+1)$ amplification matrix $\mathbf{G}$ can be extracted from system (23) by

$$\mathbf{G} = -\mathbf{BB}^{-1}\mathbf{BA} \tag{24}$$

which spectral norm is given by

$$\|\mathbf{G}\| = \sup \frac{\|\mathbf{GE}\|}{\|\mathbf{E}\|} = \sqrt{\max_i (\lambda_i(\mathbf{G}^{\mathrm{T}}\mathbf{G}))} \tag{25}$$

where $\mathbf{E}$ is an arbitrary nodal perturbation vector and λ_i the eigenvalues spectrum.

The amplification matrix for the CNG, CNTG and SUPG schemes can be found elsewhere.[20] Figure 7 displays a comparative evolution of the function $\|\mathbf{G}(Cr)\|$, for $n = 20$ (n has no significative influence on $\|\mathbf{G}\|$ as soon as $n > 10$), and indicates that the SUFG scheme has a relatively low amplification factor over the practical range of Cr number. Compared to a standard space–time approach (SUFG with $\tilde{\tilde{\alpha}}_L = 0$) and to the other schemes, the proposed method ($\tilde{\tilde{\alpha}}_L = \|\widetilde{\mathbf{\Delta s}}\|$) reverses the curvature of $\|\mathbf{G}(Cr)\|$. This contributes to explain its good performances at high Cr values.

Concerning the CNTG scheme it should be noted here that the unconditional stability, arrived at by Donea[4] using a von Neumann-type analysis, remains purely theoretical. As a matter of fact, it was empirically recognized later[5] that this scheme could not safely be used with Courant numbers ranging from slightly less to more than one. The asymptotic behavior of $\|\mathbf{G}(Cr)\|$ as Cr approaches unity ($\|\mathbf{G}(Cr=1)\| = \infty$) indeed warns for a virtual 'blowing out' of instabilities,

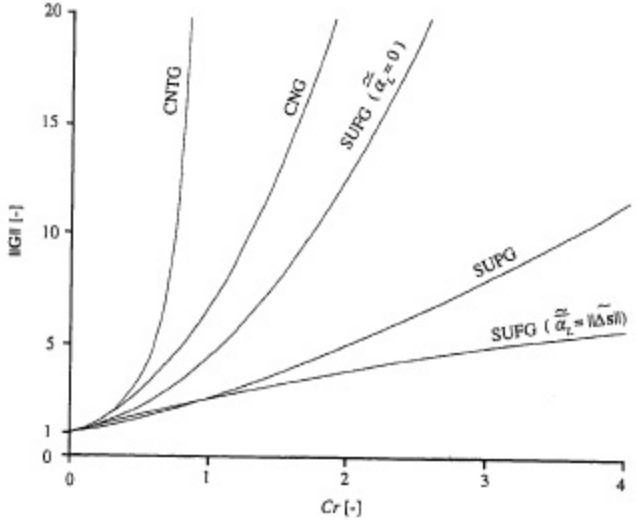

Figure 7. Norm of the amplification matrix $\mathbf{G}(Cr)$ for current schemes and for the proposed approach SUFG in the case of pure convection ($Pe = \infty$)

despite the higher orders of accuracy achieved by the CNTG scheme. Alternatively, the contemporary highly accurate Petrov–Galerkin schemes might also be affected by this phenomena which compromises the approach of practical multidimensional problems. Finally, the attention may be very shortly diverted to the striking fact that the schemes mentioned in Figure 7 always imply $\|\mathbf{G}(Cr)\| > 1$. This condition, which also prevails in diffusion–convection problems as long as the convective velocity is not zero, contradicts the classical stability criterion $\|\mathbf{G}\| \leqslant 1$.

COMPARATIVE EXAMPLES

Example 1: 1-D convective transport of a sharp front

This plug flow test problem is solved on 2-D (x, z) bi-quadratic (9 nodes) space–time elements with upstream Dirichlet boundary conditions as schematized on Figure 1. Considering the maximum sharpness given to the front (C drops from 1 to 0 over one element) and the pure convection condition ($Pe = \infty$), this problem may be seen as the most difficult. In the directions of space and time the node spacing (half element length) is $\Delta x = 0{\cdot}05$ m and $\Delta z = 1$ m. In the x direction the velocity is $v_x = 10^{-4}$ m/s and the time step $\Delta t = 400$ s is chosen, giving thus $Cr = 0{\cdot}8$ and $\beta = 1/400 = 0{\cdot}0025$ m/s (time component of the velocity $\tilde{\mathbf{v}}$). Figure 8 shows the results obtained at time $t = 20\,000$ and $80\,000$ s with the CNG, CNTG and SUPG schemes (using 1-D quadratic (3 nodes) elements and Crank–Nicholson finite difference time stepping) and with the new SUFG scheme with $\tilde{\alpha}_L = \sqrt{\Delta x^2 + \Delta z^2} \approx 1$ m.

The CNG and SUPG results exhibit the well-known difficulties relative to first-order central time stepping (downwind diffusion and upwind anti-diffusion due to second-order time-truncation errors). It can be seen that the SUPG scheme partly achieves numerical damping of the

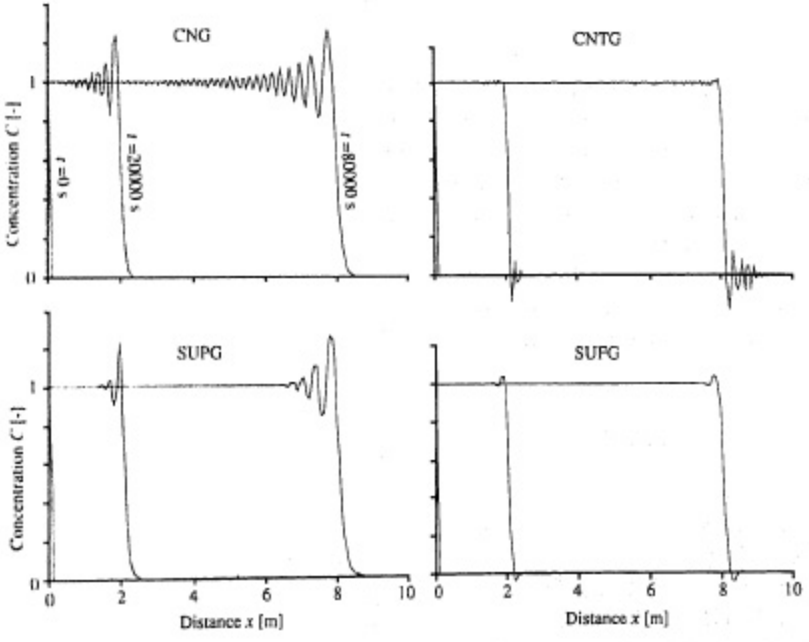

Figure 8. Convective 1-D transport of a sharp front ($Pe = \infty$, $Cr = 0{\cdot}8$). Comparison of current schemes with the proposed approach SUFG

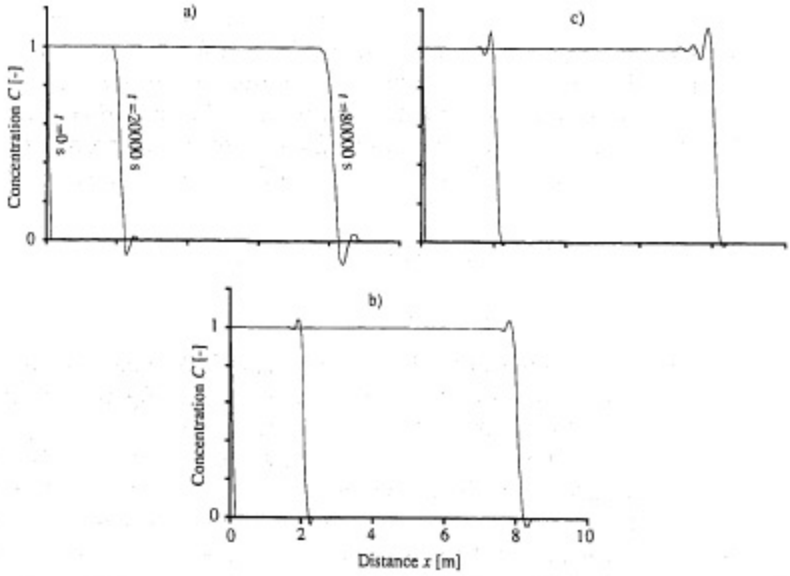

Figure 9. Convective transport of a sharp front ($Pe = \infty$, $Cr = 0{\cdot}8$). Space–time upwind effects of the SUFG scheme. (a) $\tilde{\alpha}_L = 0$, (b) $\tilde{\alpha}_L = \|\widetilde{\Delta \mathbf{s}}\|$, (c) $\tilde{\alpha}_L = 1000\ \|\widetilde{\Delta \mathbf{s}}\|$.

oscillations. However, the latter keep their frequency and the first 'peak' the same unstable amplitude (+ 25 per cent at $t = 80\,000$ s).

The results of the fourth-order accurate CNTG scheme, which takes into account the second and third order time truncation errors, show a very sharp front and a transfer of residual oscillations to the bottom of the front (− 20 per cent at $t = 80\,000$ s). On the other hand the SUFG solutions are stable with equally distributed residual oscillations of ± 3–4 per cent.

Figure 9 illustrates the net effect of parameter $\tilde{\alpha}_L$ in the SUFG scheme. When this parameter is set to zero (standard space–time finite element scheme, Figure 9(a)) the solutions exhibit a peak of negative unstable amplitude (− 14 per cent at $t = 80\,000$ s). For $\tilde{\alpha}_L = \|\widetilde{\Delta \mathbf{s}}\|$ (Figure 9(b)) irregularities are reduced and balanced immediately before and after the front. When this parameter is exaggeratedly increased (e.g. $\tilde{\alpha}_L = 1000\ \|\widetilde{\Delta \mathbf{s}}\|$, Figure 9(c)) a 'tail' appears after the front with a peak of positive unstable amplitude (14 per cent at $t = 80\,000$ s). In this latter case the fact that wiggles are created by introduction of a huge diffusivity seems very unusual. However, one has to keep in mind the space–time nature of this diffusivity which is not supposed to affect the sharpness of the front.

Example 2: 1-D convective transport of a smooth front

With data as in Example 1 the convection of a smooth front is tested. The robustness of the SUFG scheme is demonstrated by the choice of $Cr = 1{\cdot}6$ ($\Delta t = 800$ s, $\beta = 1/800$ m/s). Figure 10 compares the solutions of the CNG, SUPG, SUFG ($\tilde{\alpha}_L = 0$) and SUFG ($\tilde{\alpha}_L = \|\widetilde{\Delta \mathbf{s}}\|$) schemes at $t = 20\,000$ and $80\,000$ s. The CNTG scheme only produces overflow messages for this problem. The CNG and SUPG schemes show very similar unstable solutions. Unlike the sharp front transport problem (Figure 8) the SUPG scheme has no effect here. This last point is also verified when $Cr \leqslant 1$ and the cause of these poor performances lies in the first order Crank–Nicholson

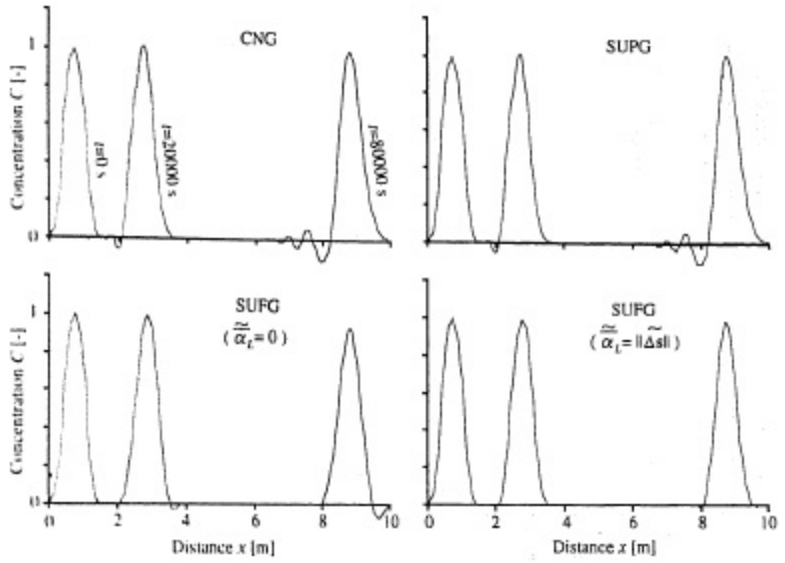

Figure 10. Convective 1-D transport of a Gaussian-type distribution ($Pe = \infty$, $Cr = 1{\cdot}6$). Comparison of current schemes with the proposed approach SUFG

time-stepping procedure used by the two schemes. The effect of parameter $\tilde{\alpha}_L$ in the SUFG scheme is also apparent in Figure 10; when it is used residual irregularities are lower than 1 per cent.

It has to be noted that in Examples 1 and 2, the SUFG scheme requests twice less solutions of the matrix system than the other schemes. Since biquadratic elements are used, the distance $\Delta z = \beta \Delta t = 1$ m (node spacing) only represents the half-width of elements in the direction of time; the total width of the space–time layer being 2 m, i.e. 1600 s.

The evolution of the SUFG solution for an increasing Courant number is shown in Figure 11, in the case of an initial front smoothed over six elements. The solution significantly deteriorates starting from $Cr = 1{\cdot}5$ due to the fact that the function $C(x, t)$ becomes too complex for the given discretization and type of elements. For $Cr = 4$ residual irregularities at $t = 80\,000$ s are $\pm$ 4–5 per cent and directly depend on the initial smearing of the front.

Example 3: 2-D convective transport in a rotating flow field

The non-dissipative qualities of the SUFG scheme are illustrated in the case of a rotating flow field involving $Cr > 1$. Figure 12(b) depicts the problem which consists in transporting a Gaussian hill along circular trajectories in the (x, y) plane. The space–time domain $(x, y, z = \beta t)$ is discretized by a layer of triquadratic elements ($32 \times 32 \times 1$, with $\Delta x = \Delta y = 1/64$ m and $\Delta z = \beta \Delta t = 1$ m) as schematized in Figure 12(a). The results in Figure 13 indicate that the peak keeps its shape and intensity during rotation. After a full rotation negative irregularities are of the order of 10^{-3} and the concentration at the centre of the peak is $C = 0{\cdot}99$. The upwind parameter used in this simulation is $\tilde{\alpha}_L = \|\widetilde{\Delta \mathbf{s}}\| = \sqrt{\Delta x^2 + \Delta y^2 + \Delta z^2} \approx 1$ m.

The peak completes a rotation in $\pi/2$ s ($\approx 1{\cdot}57$ s) and this time is divided into 50 layers representing $2\Delta t$ each, which gives $\Delta t = \pi/200$ s ($\approx 0{\cdot}0157$ s) and $\beta = 200/\pi$ m/s (≈ 64 m/s). On the trajectories transporting the peak Cr is maximum when one of the space components of the

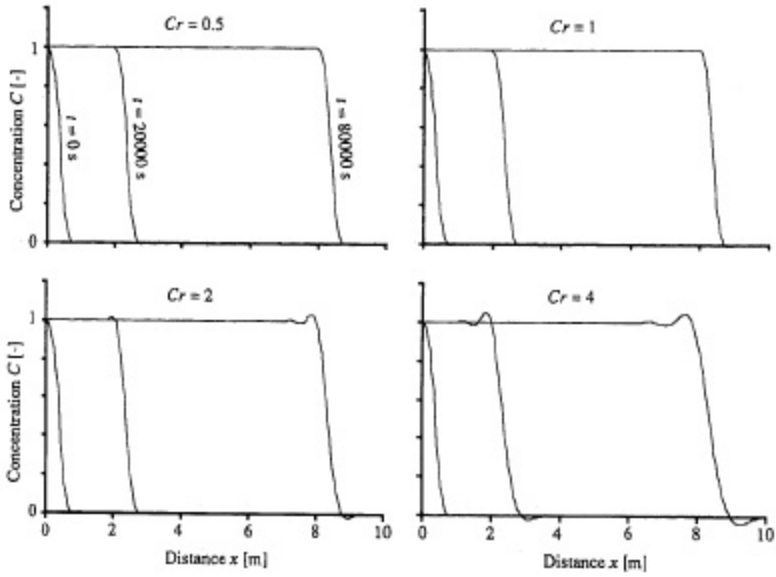

Figure 11. Convective transport ($Pe = \infty$) of a smooth front. Comparison of SUFG ($\tilde{\alpha}_L = \|\Delta \mathbf{s}\|$) solutions for an increasing Courant number (Cr)

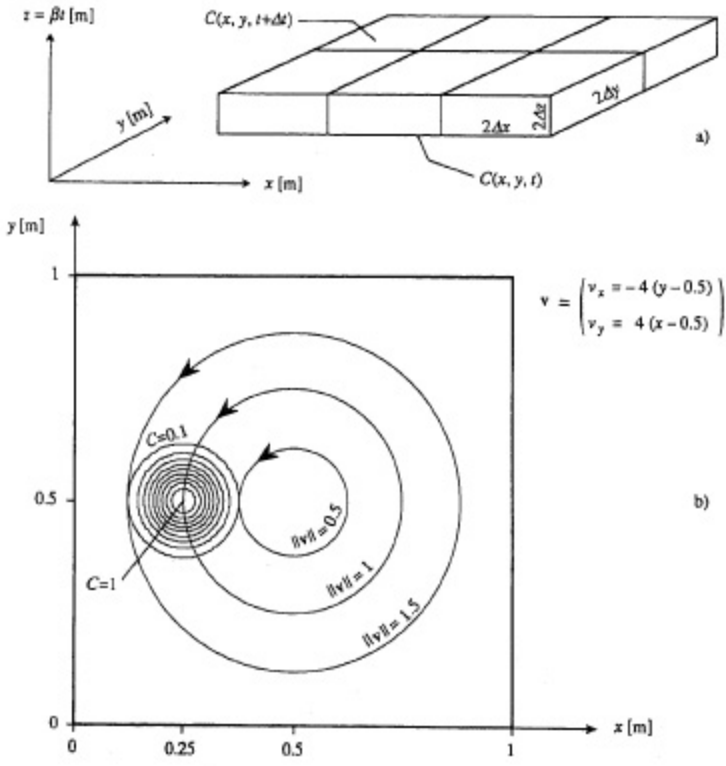

Figure 12. Convective transport ($Pe = \infty$) in a rotating flow field. (a) Space–time finite element layer. (b) Velocity field $\mathbf{v}$ and initial function $C(x, y, 0) = \exp(-\{(x - 0{\cdot}25)^2 + (y - 0{\cdot}5)^2\}/0{\cdot}007)$

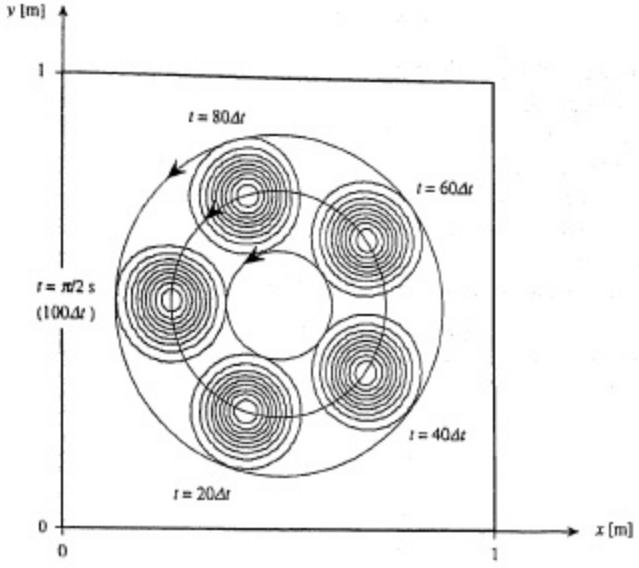

Figure 13. Convective transport ($Pe = \infty$, $Cr_{max} = 1{\cdot}5$) in a rotating flow field. $20\Delta t$ and full rotation SUFG solutions

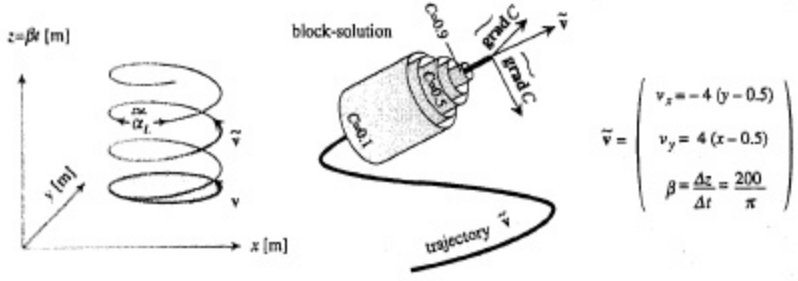

Figure 14. Space–time trajectories and block solution

velocity is zero (for example $v_x = 0$, velocity vector parallel to the y axis). Taking the multidimensional definition of Cr[14] we can then precisely calculate

$$Cr = \frac{\|\mathbf{v}\|^2 \Delta t}{|v_x||\Delta x| + |v_y||\Delta y|} = \frac{|v_y|\Delta t}{|\Delta y|} = \frac{4|x - 0{\cdot}5|64\pi}{200} = \begin{cases} 0{\cdot}5 & \text{on the interior trajectory} \\ 1{\cdot}0 & \text{on the central trajectory} \\ 1{\cdot}5 & \text{on the exterior trajectory} \end{cases}$$

In the space–time domain the fluid particles follow spring-like trajectories defined by $\tilde{\mathbf{v}}$ as shown in Figure 14. The block solution around the central trajectory in the $(x, y, \beta t)$ domain (equiconcentration surfaces) is also schematized on this figure as well as the steady-state 'perpendicularity' of $\tilde{\nabla} C$ and $\tilde{\mathbf{v}}$. The solutions reported on Figure 13 are obtained by intersecting the 3-D block-solution $C(x, y, \beta t) =$ constant with horizontal planes equidistant of $20\,\Delta t$ (20 m).

FINAL REMARKS

The robustness of a space–time Galerkin block treatment of the diffusion–convection equation was demonstrated in this work. The implementation of a stabilizing anisotropic diffusivity along space–time trajectories does not create any spacial smearing effect. The efficiency of this Streamline-Upwind-Full-Galerkin (SUFG) method is illustrated by successful solutions of deemed complex problems (infinite mesh Péclet number, Courant number exceeding unity) and performs better than other contemporary schemes in many ways. Other comparative applications and additional information can be found in References 20 and 21. In the perspective of a unified-solution procedure for various problems of mathematical physics related to hydrodynamics, research is now in progress to apply the SUFG concept to 4-D geometries and non-linear processes. This work includes the creation of a 4-D finite hyperelement library and will be reported in due course.

ACKNOWLEDGEMENTS

These new developments are made possible by the motivation of the Swiss Federal Institute of Technology (EPFL), the Swiss Academy for Technical Sciences (SATW) and the Swiss National Science Foundation (FNRS). Stimulating discussions with Prof. Jean Descloux of the Department of Mathematics at EPFL, Prof. Ghislain de Marsily at l'Ecole des Mines of Paris, France and Prof. Laszlò Kiraly of the Center for Hydrogeology at the University of Neuchâtel, Switzerland, were greatly appreciated. During the year 1990, when working at Lawrence Berkeley Laboratory (LBL), California, the author very much enjoyed the enlightening company of Dr. Jahan Noorishad who enthusiastically shared the basic idea of upwinding in the space–time domain.

REFERENCES

1. B. P. Leonard, 'A survey of finite differences of opinion on numerical muddling of incomprehensible defective confusion equation', in T. J. R. Hughes (ed.), *Finite Element Methods for Convection Dominated Flows*, AMD-Vol. 34, ASME, New York, 1979.
2. J. C. Heinrich and O. C. Zienkiewicz, 'Quadratic finite element schemes for two dimensional convective transport problems', *Int. j. numer. methods eng.*, **11**, 1831–1844 (1977).
3. A. N. Brooks and T. J. R. Hughes, 'Streamline upwind Petrov–Galerkin formulations for convection dominated flows with particular emphasis on the incompressible Navier–Stokes equations', *Comput. Methods Appl. Mech. Eng.*, **32**, 199–259 (1982).
4. J. Donea, 'A Taylor–Galerkin method for convective transport problems', *Int. j. numer. methods eng.*, **20**, 101–119 (1984).
5. J. Donea, L. Quartapelle and V. Selmin, 'An analysis of time discretization in the finite element solution of hyperbolic problems', *J. Comput. Phys.*, **70**, 463–499 (1987).
6. J. J. Westerink and D. Shea, 'Consistent higher degree Petrov–Galerkin methods for the solution of the transient convection-diffusion equation', *Int. j. numer. methods eng.*, **28**, 1077–1101 (1989).
7. T. F. Russel and M. F. Wheeler, 'Finite element and finite difference methods for continuous flows in porous media', in *The Mathematics of Reservoir Simulation*, SIAM, Philadelphia, 1983, pp. 35–106.
8. M. E. Cantekin and J. J. Westerink, 'Non-diffusive $N + 2$ degree Petrov–Galerkin methods for two-dimensional transient transport computations', *Int. j. numer. methods eng.*, **30**, 397–418 (1990).
9. J. T. Oden, 'A general theory of finite element: I; II', *Int. j. numer. methods eng.*, **1**, 205–221; 247–259 (1969).
10. G. F. Pinder and W. G. Gray, 'Galerkin approximation of the time derivative in the finite element analysis of groundwater flow', *Water. Resources Res.*, **10**, 821–828 (1974).
11. J. R. Yu and T. R. Hsu, 'Analysis of heat conduction in solids by space–time finite element method', *Int. j. numer. methods eng.*, **21**, 2001–2012 (1985).
12. J. R. Yu and T. R. Hsu, 'On the solution of diffusion-convection equations by the space–time finite element method', *Int. j. numer. methods eng.*, **23**, 737–750 (1986).
13. C. Johnson, V. Nävert and J. Pitkäranta, 'Finite element methods for linear hyperbolic problems', *Report No. 1983-4*, Chalmers Univ. of Technology and Univ. of Göeteborg, Sweden, 1983.

14. C. C. Yu and J. C. Heinrich, 'Petrov–Galerkin methods for the time-dependent convective transport equation', *Int. j. numer. methods eng.*, **23**, 883–901 (1986).
15. C. C. Yu and J. C. Heinrich, 'Petrov–Galerkin methods for multidimensional, time dependent, convection–diffusion equations', *Int. j. numer. methods eng.*, **24**, 2201–2215 (1987).
16. D. W. Kelly, S. Nakazawa, O. C. Zienkiewicz and J. C. Heinrich, 'A note on upwinding and anisotropic balancing dissipation in finite element approximations to convective diffusion problems', *Int. j. numer methods eng.*, **15**, 1705–1711 (1980).
17. T. J. R. Hughes and A. N. Brooks, 'A multi-dimensional upwind scheme with no cross-wind diffusion', in T. J. R. Hughes (ed.), *Finite Element Methods for Convection Dominated Flows*, AMD-Vol. 34, ASME, New York, 1979.
18. I. Christie, D. F. Griffiths, A. R. Mitchell and O. C. Zienkiewicz, 'Finite element methods for second order differential equations with significant first derivatives', *Int. j. numer. methods eng.*, **10**, 1389–1396 (1976).
19. D. K. Gartling, 'Some comments on the paper by Heinrich, Huyakorn, Zienkiewicz and Mitchell', *Int. j. numer. methods eng.*, **12**, 187–190 (1978).
20. P. Perrochet, 'Strategies to solve practical convection dominated transport problems using finite elements. Applications to groundwater contamination', *Ph.D. dissertation*, IATE/EPFL, Ecole Polytechnique Fédérale de Lausanne, Switzerland, 1992.
21. P. Perrochet, A. Musy, J. Noorishad and C. F. Tsang, 'An improved methodology for the solution of convection dominated solute transport problems', in *Proc. ISRM Conf. on Fracturated and Jointed Rock Masses*, Lake Tahoe, 1992.